

Fast nanofluidics by travelling surface waves

Jian-Fei Xie¹ · Bing-Yang Cao¹

Received: 28 November 2016 / Accepted: 6 June 2017
© Springer-Verlag GmbH Germany 2017

Abstract In this paper, we investigate the fast flow in nanochannels, which is induced by the travelling surface waves. The nanoscale fluid mechanism in nanochannels has been influenced by both amplitude and frequency of travelling surface waves, and the hydrodynamic characteristics have been obtained by molecular dynamics simulations. It has been found that the flow rate is an increasing function of the amplitude of travelling surface waves and can be up to a sevenfold increase. However, the flow rate is only enhanced in the limited range of frequency of travelling surface waves such as low frequencies, and a maximum fivefold increase in flow rate is pronounced. In addition, the fluid–wall interaction (surface wettability) plays an important role in the nanoscale transport phenomena, and the flow rate is significantly increased under a strong fluid–wall interaction (hydrophilicity) in the presence of travelling surface waves. Moreover, the friction coefficient on the wall of nanochannels is decreased obviously due to the large slip length, and the shear viscosity of fluid on the hydrophobic surface is increased by travelling surface waves. It can be concluded that the travelling surface wave has a potential function to facilitate the flow in nanochannels with respect to the decrease in surface friction on the walls. Our results allow to define better strategies for the fast nanofluidics by travelling surface waves.

Keywords Travelling surface wave · Nanofluidics · Fast flow · Molecular dynamics

✉ Bing-Yang Cao
caoby@tsinghua.edu.cn

¹ Key Laboratory for Thermal Science and Power Engineering of Ministry of Education and Department of Engineering Mechanics, Tsinghua University, Beijing 100084, China

1 Introduction

During the past two decades, we see the fast development and wide applications of nanotechnologies such as micro-/nanoelectromechanical systems (MEMS/NEMS) Ho and Tai (1996), Ho and Tai (1998), Gad-el-Hak (1999), Cao et al. (2009), biological chips and lab-on-a-chip Daw and Finkelstein (2006), Craighead (2006), Ding et al. (2013), Bocquet and Tabeling (2014). Nanoscale transport governs the behaviour of a wide range of nanofluidic systems, but it remains less understood due to the enormous hydraulic resistance associated with the nanoconfinement and the resulting minuscule flow rates in MEMS/NEMS. As a point of long-standing view, it is of great importance pursued by many researchers due to its implications in mass and momentum transport at micro-/nanoscales, and the micro-/nanoflow control is also important for practical applications: DNA profiling Insepov et al. (2006), optical filters and display technology Cecchini et al. (2008), thermal management of semiconductor elements and pollution monitoring Roosta et al. (2016). However, the huge surface–volume ratio up to $10^6 - 10^9$ significantly affects the mass and momentum transport in micro-/nanoelements and makes this type of research challenging.

Obviously, the challenge is to overcome the large surface and viscous forces that prevent the fluid from flowing at the nanoscale, wherein other driving forces can be ignored in most microfluidic systems Yeo and Friend (2009), Friend and Yeo (2011), Arash et al. (2015). There is no doubt that the inertia becomes significant in nanofluidic flows and results in the low efficiency of mass transport. Thus, fast flow in nanochannels and large flow rate are highly appreciated. Traditional approaches to reduce the skin friction and increase the flow rate are the use of hydrophobic or

nanostructured surfaces in micro-/nanochannels Cao et al. (2006a), Liakopoulos et al. (2016). For the case of macroscopic flows, most structured fluids of polymeric and/or multiphase nature encountered in industrial practice exhibit shear-thinning behaviour, and vibrating pipes can result in the fluidity of such material and hence facilitate its processing Kazakia and Rivlin (1978), Kazakia and Rivlin (1979), Piau and Piau (2002). In addition, it has been found in tribological field that mechanical vibrations affect frictional sliding and the associated stick–slip patterns that cause a drastic reduction in the friction force somehow Capozza et al. (2009). These findings have useful applications in nanotribology and help to understand earthquake triggering by small dynamic perturbations. However, it seems less feasible to apply the mechanical vibration to the microfluidics and nanofluidics due to the small scales, and the micro-/nanoelements may be damaged under the mechanical vibrations. On the other hand, the travelling waves have been widely applied to the nanoscale confinements such as the enhancement of mass flow rate in carbon nanotubes Guttenberg et al. (2004) and nanopumping phenomena Zhou et al. (2015).

In microfluidic biochip engineering, a driving force for driving microscale fluid motion has been introduced by employing the surface waves Koster (2007), Cecchini et al. (2008), Mao et al. (2016). The key of this novel technology is to make a micropump that is able to position reagents on the surface of chips or in microfluidic channels without the mechanical contact. This is implemented in terms of the surface acoustic waves (SAW) that are induced using radio frequency electric signals. These waves arise through the use of piezoelectric substrate materials in the chip, e.g. lithium niobate Cecchini et al. (2008). This electromagnetic signal is efficiently converted into an elastic wave propagating on the surface layer of the substrate, i.e. SAW. In recent years, SAW technologies have been attractive and received significant attention in microfluidics and nanofluidics community: biological/chemical sensing Guo et al. (2014), micro-/bioparticle manipulation schemes and on-chip droplet production Brenker et al. (2016). It is interesting that the SAW-induced effect has similarity in live nature, for example with the skin features of fast-swimming sea animals, such as dolphins Insepov et al. (2006). Their findings indicate that dolphins use travelling waves on their skin surface to damp the turbulence in the boundary layers near the skin surface. Investigators have demonstrated that SAWs can be efficiently used to control fluids and particles in lab-on-a-chip devices Ding et al. (2013), Zhou et al. (2014), Nama et al. (2015).

The properties of nanoconfined liquids have been the object of much interest. For example, Bocquet and

Jean-Louis studied the dynamical properties of fluids confined at molecular scales and investigated the influence of confinement on the self-diffusion coefficient in a fluid slab Bocquet and Barrat (1996). Particularly, nanoscale confinements may induce significant changes in liquid viscosity. As a result, constitutive laws, boundary conditions and transport in nanoscales may significantly deviate from those used in the Navier–Stokes (NS) equations and need extensive investigations in terms of atomistic approaches. In the past two decades, molecular dynamics (MD) simulations have emerged as a powerful tool for probing the microscopic behaviour of fluids at the molecular level Koplik and Banavar (1995), Barisik and Beskok (2011), Liang and Ye (2014). Very recently, a phenomenological continuum model has been developed using systematic MD simulations of force-driven flows confined in nanochannels. Combined with their observations of constant slip length and kinematic viscosity, the model can accurately predict the velocity distribution and volumetric and mass flow rates in different height nanochannels Ghorbanian et al. (2016). On the other hand, Bhadauria and Aluru proposed a quasi-continuum hydrodynamic model for isothermal transport of Lennard-Jones fluid confined in slit-shaped nanochannels. The proposed hydrodynamic model yielded a good agreement of velocity profiles obtained from non-equilibrium MD simulations for gravity-driven flow Bhadauria and Aluru (2013). Furthermore, a quasi-continuum self-diffusion theory was introduced to capture the ordering effects and the density variations that were predicted by non-equilibrium MD in nanochannel flows, which can be seen as an alternative to the atomistic simulation Giannakopoulos et al. (2014). Interestingly, two kinds of external perturbing forces, i.e. sinusoidal and step pulse, were applied on the Poiseuille flow through a nanochannel using non-equilibrium MD simulations, and the velocity profiles reached a good agreement with the NS solutions Ziarani and Mohamad (2006).

In this paper, our purpose is to present that the travelling surface waves propagating on the walls of nanochannels can offer a powerful method for inducing a host of extremely fast nanofluidic flow. Moreover, the mass transport mechanism at the nanoscale will be explored and large flow rates in nanochannels can be expected. The rest of the work is organized as follows. In Sect. 2 an external force-driven nanochannel flow and MD techniques are introduced, and the application of travelling surface waves is also described. The nanoscale hydrodynamics of fluid flowing through nanochannels in the presence of travelling surface waves is investigated in Sect. 3. We draw our conclusions in Sect. 4.

2 Methodology and simulation details

2.1 Force-driven flow

A three-dimensional Poiseuille flow has been carried out to investigate the fast flow in the nanochannel, and the fluid is confined between two solid planar walls parallel to the xy plane with periodic boundary conditions imposed along the x and y directions, which is shown in Fig. 1. Poiseuille flow is driven by a pressure gradient along the x direction and is locally fully developed (LFD) to be laminar with small Reynolds numbers. In the case of the planar Poiseuille flow of a Newtonian fluid under constant external force, the macroscopic hydrodynamics gives a parabolic solution of the NS equations. Considering the slip boundary condition, the velocity profile of a LFD flow may be written as Morris et al. (1992)

$$u_x = \frac{\rho g}{\mu} \left(z - \frac{H}{2} \right)^2 + \left[u_s - \frac{\rho g H^2}{8\mu} \right], \quad (1)$$

in which H is the distance between the two walls of the nanochannel, ρ is the density of the fluids, μ is the dynamical viscosity, u_s is the slip velocity at the fluid–solid boundary, and g is the acceleration factor. According to the Navier boundary condition, the slip length can be calculated by extrapolating the velocity profiles from the position in the fluid to where the velocity would vanish. In our previous MD simulations Xie and Cao (2016), Xie and Cao (2017), the slip length L_s is computed by Thompson and Troian (1997), Gad-el-Hak (1999)

$$L_s = \frac{u_s}{\partial u / \partial z}. \quad (2)$$

Note that the walls are located at $z = 3.5\sigma$ and $z = 21.5\sigma$ (σ is the molecular diameter of fluid molecules), respectively, and Eq. (1) is applicable for the current external force-driven flow by locating the central line of flows in the middle of the nanochannel. Now we focus on the solid walls, each of which consists of atoms forming two planes of a face-centred cubic (f.c.c) lattice. To maintain a well-defined solid structure with a minimum number of solid atoms, each wall atom is attached to a lattice site with a spring. Based on the Einstein theory, each wall atom vibrates around the f.c.c lattice site with the Einstein frequency by a harmonic spring with stiffness

$$\kappa = 16\pi^4 k_B^2 m \theta^2 / \hbar^2, \quad (3)$$

where k_B and \hbar are the Boltzmann and Plank constants, m is the mass of a wall atom, and $\theta = 180$ K is the Einstein temperature Cao et al. (2005). The spring constant is used to control the thermal roughness of the wall and its responsiveness to the fluid. The simulated characteristic length, i.e. the distance between the two plates, reaches $H = 18\sigma$, which is really comparable with the characteristic size of MEMS devices in engineering situations. The sizes of the simulation cell in the x and y directions are $L_x = 37\sigma$ and $L_y = 14.3\sigma$, respectively. In particular, the travelling surface wave is generated and propagates on the walls of nanochannels along the x direction. The travelling surface wave, i.e. the perturbation to the wall atoms, is governed by Worden (2001)

$$A = A_0 \cos(\omega t - kx), \quad (4)$$

in which A_0 , $\omega = 2\pi/T$ and T are the amplitude, frequency and period of the travelling surface wave, respectively. Parameter k corresponds to the spatial frequency of the travelling surface wave and is related to the wavelength λ by $k = 2\pi/\lambda$ (wavenumber $\nu = 1/\lambda$). Since the present investigations focus on the Rayleigh surface travelling wave, the longitudinal component of the displacement is given only. In addition, the exponential decay of transverse displacement is negligible due to the small size of nanochannel, and the original form of Rayleigh wave is reduced to Eq. (4). It can also be concluded that the perturbation of wall atoms is exactly governed by Eq. (4) and follows the form of Rayleigh surface travelling wave. In order to impose the travelling surface wave correctly, a proper phase velocity, i.e. $\omega\lambda/2\pi$, should be chosen to guarantee $N\lambda$ on the walls of nanochannel, where N is a positive integer. The ranges of travelling wave parameters that are used in our MD simulations are listed in Table 1.

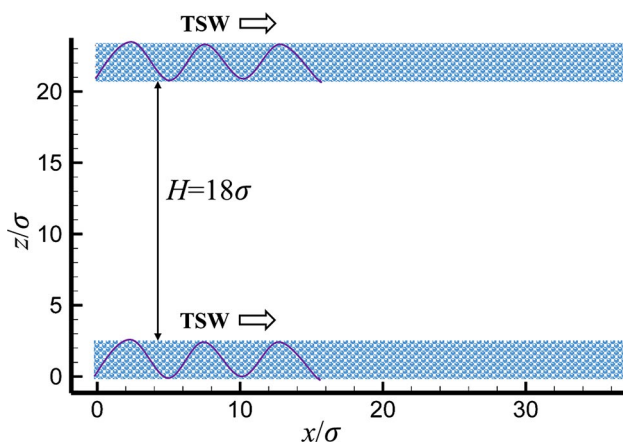


Fig. 1 Schematic of nanochannel flow in the presence of travelling surface wave: channel length $L_x = 37\sigma$ and channel height $H = 18\sigma$. The y direction points into the xz plane, and the length of cell in the y direction is $L_y = 14.3\sigma$. The travelling surface waves propagate on the walls of nanochannel along the positive direction of x axis

Table 1 Physical parameters in MD simulations

| Parameter | Symbol | Value |
|--------------|--|------------------------------|
| Diameter | σ_A | 3.405×10^{-10} m |
| | σ_{AP} | 3.085×10^{-10} m |
| Energy | ε_A | 1.67×10^{-21} J |
| | ε_{AP} | 0.894×10^{-21} J |
| Mass | m_A | 40 a.u. |
| | m_P | 195 a.u. |
| Time | $\tau = \sigma_A \sqrt{m_A/\varepsilon_A}$ | 2.15×10^{-12} s |
| Temperature | ε_A/k_B | 119.8 K |
| Density | ρ | $0.8 m_A/\sigma_A^3$ |
| Amplitude | A_0 | $0.01-0.05 \sigma_A$ |
| Frequency | ω | $2-1000 \tau^{-1}$ |
| Wavelength | λ | $0.1-10 \sigma_A$ |
| Wavenumber | ν | $0.1-10 \sigma_A^{-1}$ |
| Acceleration | g | $0.01-0.025 \sigma_A/\tau^2$ |

2.2 Molecular dynamics

The fluids confined between the two planar plates are chosen as liquid argon in our MD simulations, and molecules interact through a Lennard-Jones (LJ) potential

$$\phi(r_{ij})^{LJ} = \begin{cases} 4\varepsilon \left[\left(\frac{\sigma}{r_{ij}} \right)^{12} - \left(\frac{\sigma}{r_{ij}} \right)^6 \right], & r_{ij} \leq r_c \\ 0, & r_{ij} > r_c \end{cases} \quad (5)$$

where r_{ij} is the intermolecular distance, r_c is the cutoff distance, and ε is the energy parameter, respectively. For the argon–argon interaction, $\sigma_A = 3.405 \times 10^{-10}$ m is chosen as a length unit and $\varepsilon_A = 1.67 \times 10^{-21}$ J is applied as an energy unit. The fluid–wall (argon–platinum) interaction is also modelled with the Lennard-Jones (LJ) potential and is expressed as follows

$$\phi(r_{ij})_{AP} = 4c\varepsilon_{AP} \left[\left(\frac{\sigma_{AP}}{r_{ij}} \right)^{12} - \left(\frac{\sigma_{AP}}{r_{ij}} \right)^6 \right], \quad (6)$$

in which the constant c is used to control the interaction strength between the fluid molecules and wall atoms, i.e. surface wettability, and larger values of c refer to the stronger interactions between fluid molecules and wall atoms (hydrophilic surface). Three magnitudes of fluid–wall interaction (FWI), i.e. $c = 0.25$, $c = 0.5$ and $c = 1.0$ are considered in our MD simulations, where $c = 0.25$ refers to a weak FWI (hydrophobicity). The length and energy scales $\sigma_{AP} = 3.085 \times 10^{-10}$ m and $\varepsilon_{AP} = 0.894 \times 10^{-21}$ J are obtained in terms of Lorentz–Berthelot rule Allen and Tildesley (1987), Rapaport (1995). The molecular mass for argon is $m_A = 40$ a.u. and for platinum $m_P = 195$ a.u., and the natural time unit in MD runs is chosen as

$\tau = \sigma_A \sqrt{m_A/\varepsilon_A} = 2.15 \times 10^{-12}$ s. It should be noted that all dimensional quantities such as the fluid density ρ and velocity u given by the LJ unit in our MD simulations will be understood to be multiplied by an appropriate combination of σ_A , ε_A and m_A , which is also shown in Table 1.

The fluid molecules move according to Newton's second law, and the equations of motion are integrated using a leapfrog Verlet algorithm with a time step of $\Delta t = 0.002\tau$. To reduce the time-consuming part of the calculation of intermolecular interactions, we take two main measures: a typical potential cutoff of $r_c = 2.5\sigma$ is shifted, and the cell-linked list method is adopted Allen and Tildesley (1987). The equilibrium state of the fluid is well-defined liquid phase characterized by number density $\rho = 0.8\sigma^{-3}$ and temperature $T = 1.1k_B/\varepsilon_A$. The number of fluid molecules and wall atoms is 5292 and 1600, respectively. The velocity rescaling technique is applied to wall atoms to maintain a constant wall temperature which is same as the fluid temperature.

The motion equation of the i th molecule is

$$m \frac{dz_i^2}{dt^2} = \sum_{j \neq i} \frac{\partial \phi^{LJ}}{\partial z_i} - m\Gamma \dot{z}_i + \eta_i, \quad (7)$$

where Γ is a friction constant determining the rate of heat exchange between the simulation system and the heat reservoir, and η_i is a Gaussian distributed random force Grest and Kremer (1986). Particularly, the force-driven flow is implemented by adding the acceleration factor g to each fluid molecule along the flow direction while calculating the velocity. The fluid system is kept at a constant temperature by a Langevin thermostat method in the z direction Thompson and Robbins (1989). We ensure that the velocity shear rate at the boundary of nanochannel flows is much smaller than the critical value $\dot{\gamma} \sim (m\sigma_{AP}^2/\varepsilon_{AP})^{-1/2}$, and thus, it can be guaranteed that the slip length at the boundary is independent of the driving field in our MD simulations Thompson and Troian (1997). A typical computation in our MD simulations requires 1,000,000 time steps to reach the steady flow state. We spend about 1,500,000 additional time steps on averaging the macroscopic characteristics, and the number of bin is equal to twice the number of unit cells of the initial FCC lattice giving a bin width $O(\sigma)$ Koplik et al. (1989).

3 Results and discussion

First of all, we investigate the fluid flow in nanochannels to verify our MD solver. In this case, the same nanochannel that is shown in Fig. 1 is chosen, but the travelling surface wave has been only imposed on the bottom wall. We

compare the flow under the travelling surface wave with a base flow without applying the surface wave. For the base flow, which is shown in Fig. 2a, two condensed fluid layers

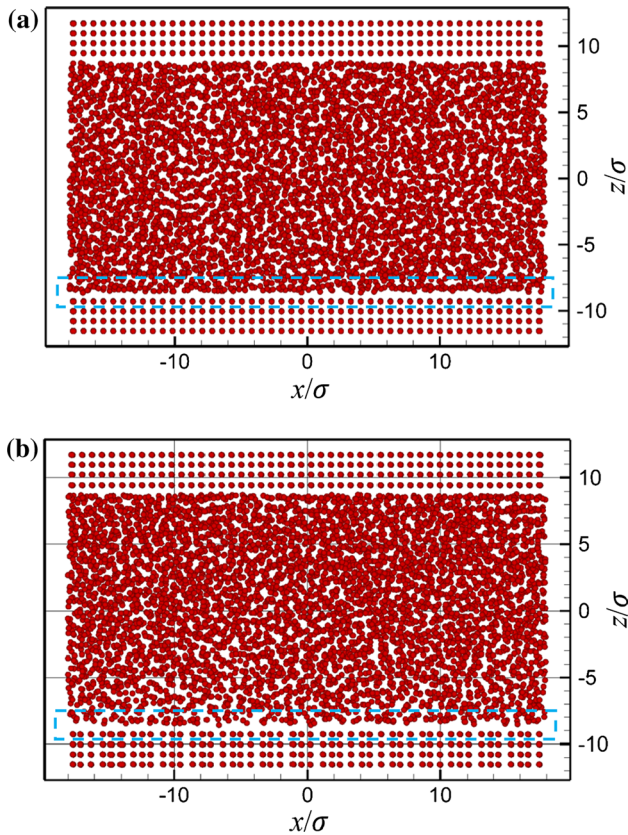
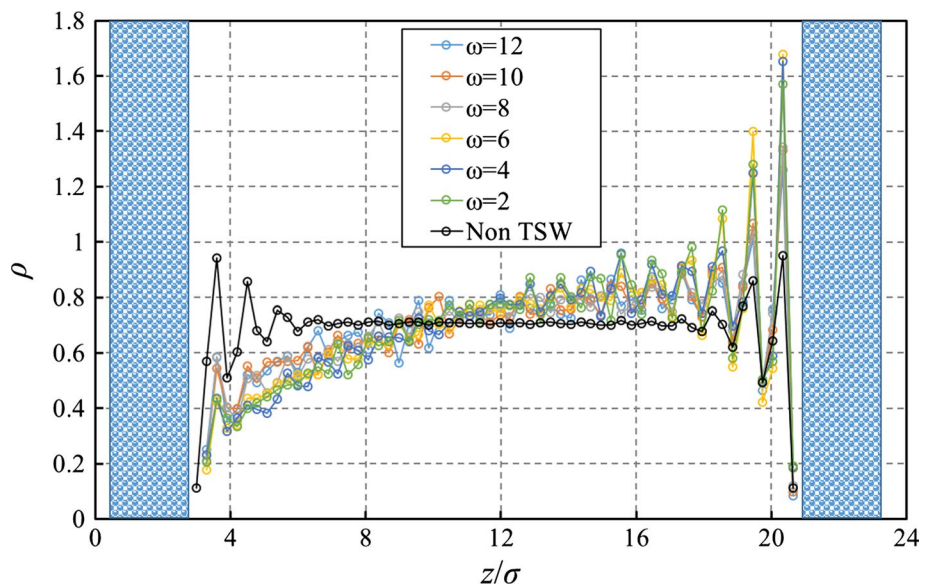


Fig. 2 Flow patterns in nanochannels: **a** steady flow without the travelling surface wave and **b** the travelling surface wave-induced flow. The blue dotted rectangular box indicates the molecular behaviours near the wall: molecular layering (a) or not (b) (color figure online)

Fig. 3 Density profiles under the different frequencies of travelling surface waves in the nanochannel



that are called “solid-like liquid” (framed by the blue rectangular box) are constructed near both top and bottom walls due to the interactions between fluids and solid wall. As shown in Fig. 2b, however, the condensed fluid layer near the bottom wall is disappeared due to the propagation of travelling surface wave on the bottom wall (also framed by the blue rectangular box). Therefore, we expect that the profile of fluid density near the bottom wall may be affected by the travelling surface wave, and the density profile of fluid across the nanochannel is shown in Fig. 3. It is shown in Fig. 3 that the oscillation of fluid density near the bottom in the presence of travelling surface waves is obviously reduced in comparison with the base flow without applying the surface wave. This observation is consistent with the disappearance of condensed fluid layer shown in Fig. 2b. Moreover, the fluid density is increased along the height of nanochannel and the oscillation of fluid density near the top wall is fiercer compared to the base flow. Besides, the frequency of travelling surface waves is in the range of 2–10, and it is found that the density profiles are slightly affected by the low frequencies of travelling surface waves. It has also been reported that SAWs produced by the interdigital transducer (IDT) can provide an effective approach to pump fluids through microchannel arrays at ultra-high frequencies Shilton et al. (2014), and we will discuss this issue later.

We focus on the dynamic characteristics of fluid flowing through nanochannels under the travelling surface wave, and the velocity field of nanochannel flow is shown in Fig. 4. As shown in Fig. 4, the fluid is driven along the propagation direction of the travelling surface wave and a streaming phenomenon is observed when a travelling surface wave is applied to the bottom wall of the nanochannel. In addition, the velocity profiles are shown in Fig. 5

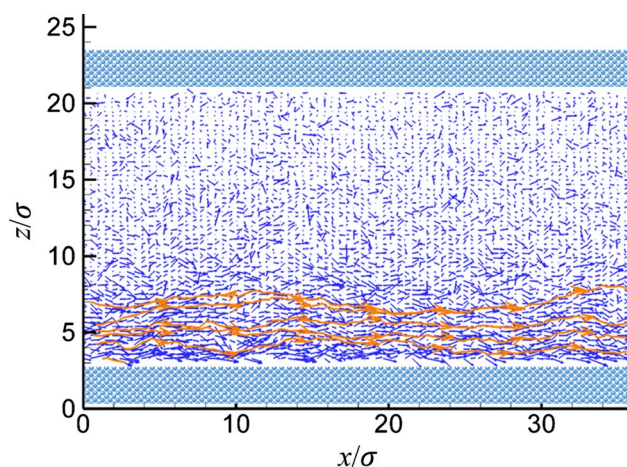
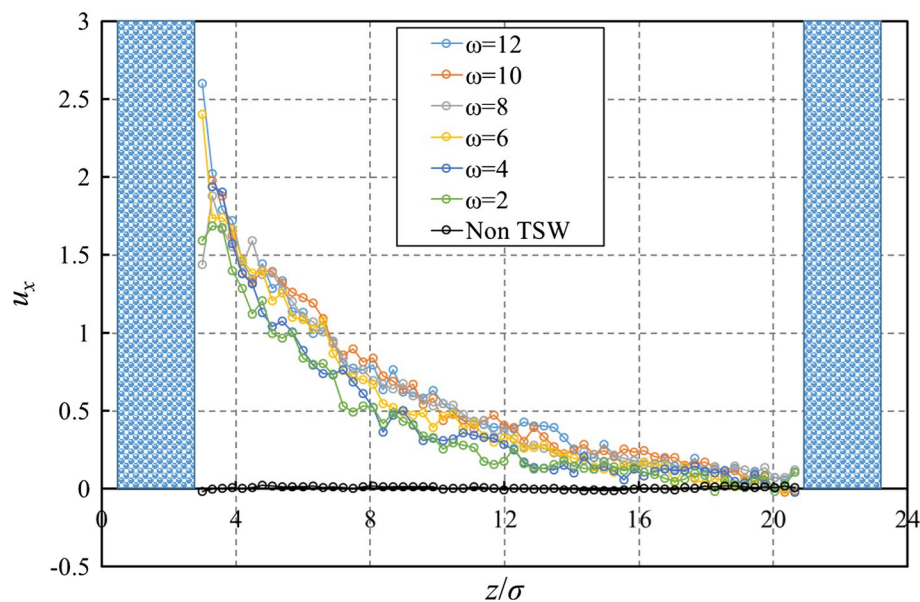


Fig. 4 Velocity field of fluid flowing through the nanochannel induced by the travelling surface wave. The orange solid lines indicate the streamlines of fluid flow near the bottom wall

indicating a power law relationship along the height of nanochannel, i.e. $u_x = bz^a$, where a and b are fitting constants. Yeo and Friend had observed that the streaming velocities achieved by SAW can reach 1 cm/s, which is much larger than that obtained by electrokinetic micropumps Yeo and Friend (2009). It is also shown in Fig. 5 that the influence of travelling surface waves on the velocity profiles in the nanochannel is insignificant under the low frequencies, including the frequencies ranged from 2 to 12, and no flow is observed in the nanochannel in the absence of the travelling surface wave. Comparing the nanochannel flow caused by the travelling surface with the base flow, we conclude that the present MD solver enables us to impose the travelling surface wave on the walls of nanochannels,

Fig. 5 Velocity profiles under the different frequencies of travelling surface waves in the nanochannel plotted with the one in the absence of travelling surface wave (black open circles)



and its effect on the nanoscale fluid dynamics can also be explored.

The attentions should be paid to the effect of travelling surface waves on the nanochannel flows, such as amplitude and frequency. As discussed in Sect. 2, the force-driven Poiseuille flow in nanochannels is chosen as the test flow in our investigations, and the travelling surface waves have been imposed on the walls of nanochannels. The first character that is considered is amplitude, and the effect of vibration amplitude on the flow in nanochannels is shown in Fig. 6, in which the values for amplitude of vibration are set as $u_0 = 0.01, 0.02, 0.03, 0.04$ and 0.05 , respectively, and $\omega = 10$, $c = 0.25$ and $g = 0.01$. It should be noted that filled symbols correspond to the cases with applying the travelling surface waves on the walls of nanochannels and open ones to cases in the absence of travelling surface waves. The following simulation results will be discussed in the same way. As shown in Fig. 6, the flow velocity across the nanochannel has been increased with the increase in the vibration amplitude compared to that in the absence of travelling surface wave. In addition, the velocity profile gets flat as the amplitude of vibration increases. For example, the velocity profile approaches perpendicular to the walls of nanochannels under the large amplitude of vibration, i.e. $u_0 = 0.05$. Moreover, the velocity slip has been observed on the walls of nanochannels in the presence of travelling surface waves, and the slip length gets increased as the amplitude of vibration increases, which is shown in Fig. 6. The phase velocity of travelling surface waves may also affect the fluid slip on the wall, and the effect is shown in Fig. 7. As shown in Fig. 7, the slip length is decreased as the increment in the phase velocity of travelling surface waves. Wide velocity profiles refer to as large average

Fig. 6 Effect of amplitude of travelling surface waves on velocity profiles. Filled symbols correspond to the cases with applying the travelling surface waves on the walls of nanochannels and open ones to the case in the absence of travelling surface waves

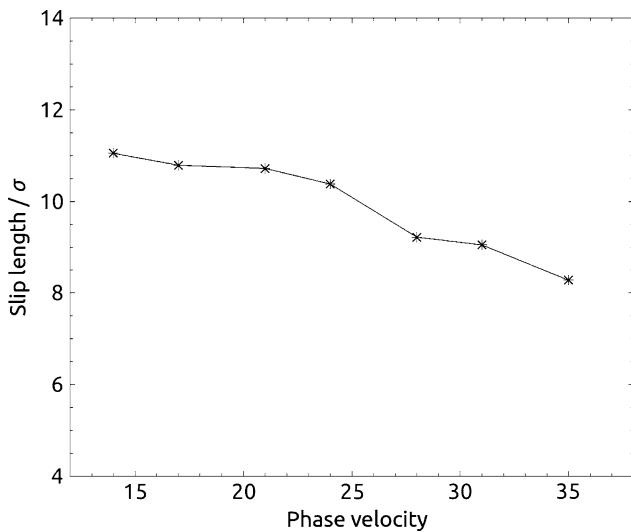
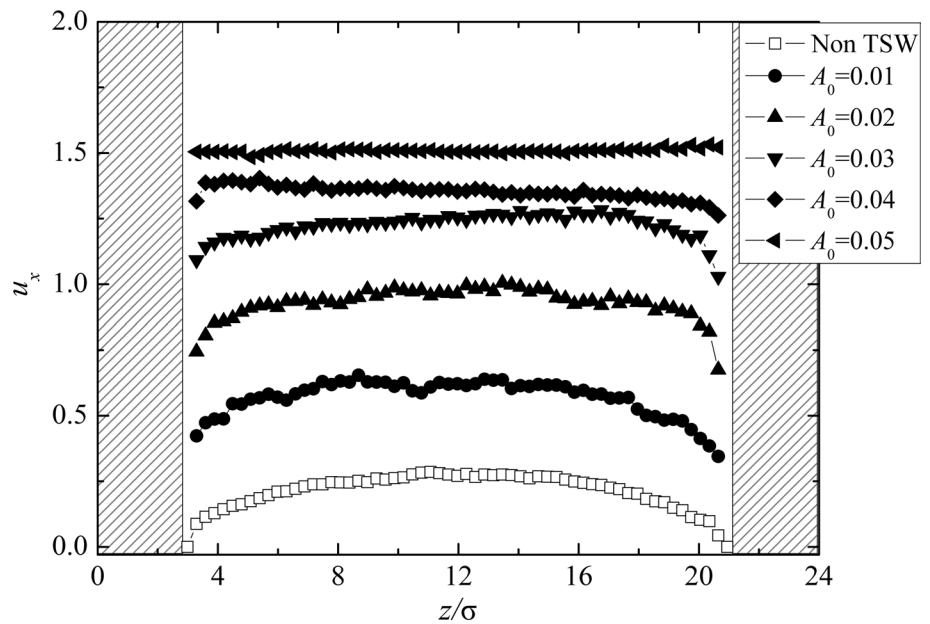


Fig. 7 Slip length of the fluid on the wall as a function of the phase velocity of travelling surface waves with $A_0 = 0.01$

flow velocities across the nanochannels, and accordingly the flow rate ratio is shown in Fig. 8 with respect to the base flow rate in the absence of travelling surface wave. The flow rate ratio is seen unity without imposing the travelling surface wave on the walls of nanochannels and is increased linearly with the amplitude of vibration. However, the increase slows down when the amplitude of vibration reaches 0.03. It is concluded in Fig. 8 that the flow rate in nanochannels in the presence of travelling surface waves can be enhanced up to 7.0 times larger than the base flow and the increase slows down at large amplitudes of vibration. In addition, the thermodynamic properties of fluids in the nanochannel were monitored, and the spatial

distribution of temperature and pressure is shown in Figs. 9 and 10, respectively. Figure 9 indicates that the temperature of fluids is kept about the initial value in spatial distribution under different conditions (with/without applying travelling surface waves). The stress tensor is calculated using the Irving–Kirkwood expression Irving and Kirkwood (1950), in which the interaction between fluid molecules is taken into account, and it is shown in Fig. 10. As shown in Fig. 10, the total stress of nanochannel flow under the surface waves travelling on the walls is smaller than that in the absence of travelling surface wave.

Apart from the amplitude, the effect of frequency of travelling surface waves on the flow in nanochannels is also essential, which is shown in Fig. 11, and the following values for frequency of vibration are chosen: $\omega = 10, 50, 100, 300, 400, 500$ and 1000 along with $u_0 = 0.01, c = 0.25$ and $g = 0.01$. Obviously, the flow velocity in the nanochannel has been increased as the frequency of vibration increases in comparison with that in the absence of travelling surface waves. However, the increase in flow velocity in the nanochannel holds on at $\omega = 300$. Moreover, the flow velocity drops when the frequency of vibration approaches 400, and is slightly higher than that in the absence of travelling surface waves as the frequency of vibration increases to 1000. The velocity slip also occurs in the presence of travelling surface waves with respect to different frequencies. However, the no-slip boundary condition is observed at high frequency of travelling surface waves such as $\omega = 500$ and $\omega = 1000$. The influence of frequency of travelling surface waves on the nanochannel flows is complicated, and a variety of flow rate ratio as a function of frequency is shown in Fig. 12. It is shown in Fig. 12 that the flow rate of fluid under low frequencies

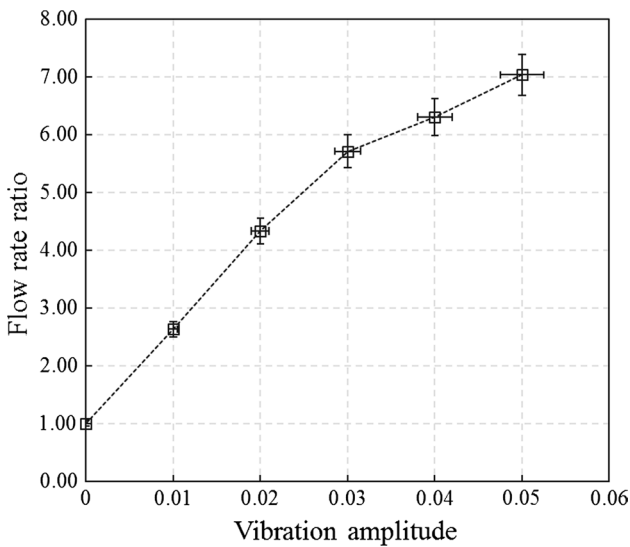
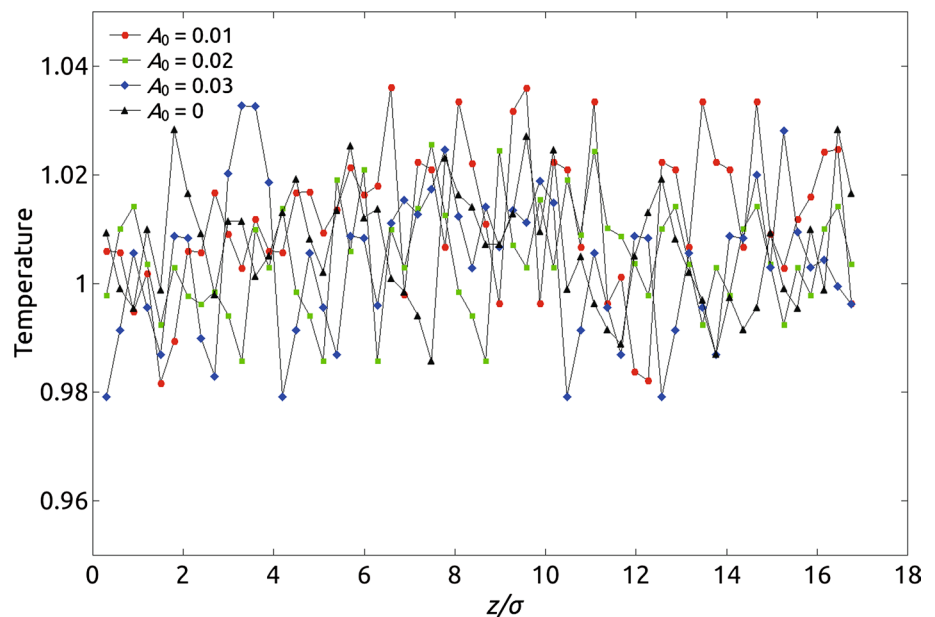


Fig. 8 Flow rate ratio as a function of amplitude of travelling surface waves

in the nanochannel is increased sharply to 5 times larger than that without applying the travelling surface wave, but is enhanced slightly after the frequency reaches 50. It is interesting that the flow rate is not increased monotonously as the increase in frequency and is insensitive to the low frequencies. In contrast, the flow rate starts to drop down when the frequency of travelling surface waves goes up to 300. Furthermore, the flow rate of fluid in the nanochannel falls significantly as the frequency exceeds 500, and keeps the level as that in the absence of travelling surface waves. It can be concluded that the flow rate of fluid in the nanochannel can be enhanced in the limited range of frequency

Fig. 9 Spatial distribution of the fluid temperature across the nanochannel



of travelling surface waves such as low frequencies. Shilton et al. (2014) also demonstrated that the microchannel flow features scale down with the increase in frequency, and they suggested that SAWs systems can be integrated into portable and complex biochip devices by carefully choosing the operating frequencies.

As the external force-driven flow is considered in our investigation, i.e. the acceleration field of $g = 0.01, 0.015, 0.02$ and 0.025 is taken into account ($u_0 = 0.01, \omega = 10$ and $c = 0.25$), and the velocity profiles of fluid in nanochannels as a function of the acceleration factor under travelling surface waves are compared to the cases without applying travelling surface waves, which are shown in Fig. 13. It is shown in Fig. that the flow velocity is increased with the increment in the acceleration whether the travelling surface wave is imposed on the walls of nanochannels or not, which is consistent with that the average velocity of fluid is proportional to the acceleration. In addition, the velocity slip occurs on the walls of nanochannels for all flows in the presence of travelling surface waves no matter how small the magnitude of acceleration is. The average flow velocities are all increased by travelling surface waves, and the flow rate ratio is shown in Fig. 14. It is obviously shown in Fig. 14 that the flow rate ratio is a decreasing function of the acceleration in nanochannels, and the ratio is reduced from 5 to 2 times as the acceleration increases from 0.01 to 0.025. It can be concluded that the flow rate has been enhanced significantly under the small acceleration in the presence of travelling surface waves in comparison with that under the large acceleration.

As mentioned earlier, the fluid–wall interaction (FWI), i.e. surface wettability, also plays an important role in the mass and momentum transport of fluid at micro-/

Fig. 10 Spatial distribution of the fluid pressure across the nanochannel

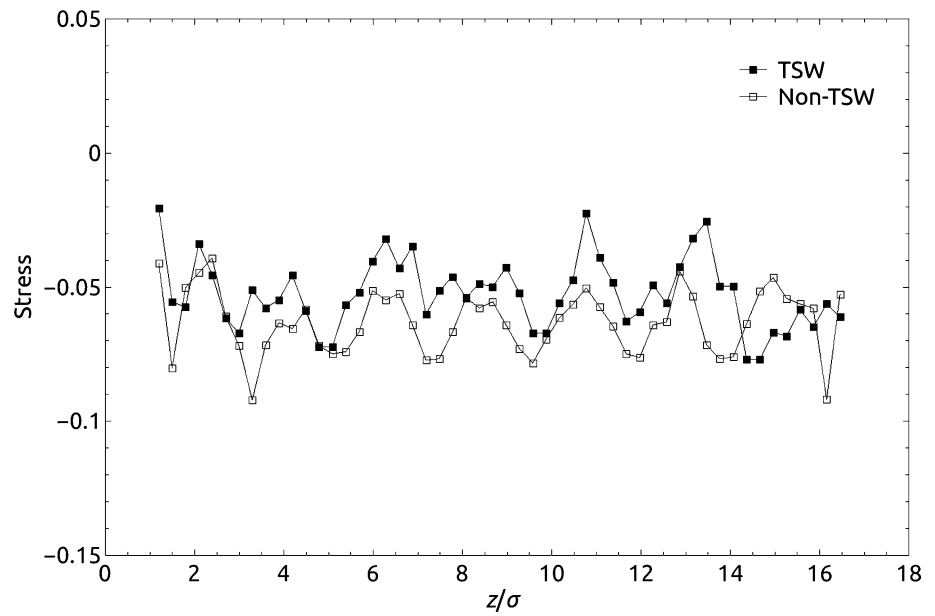
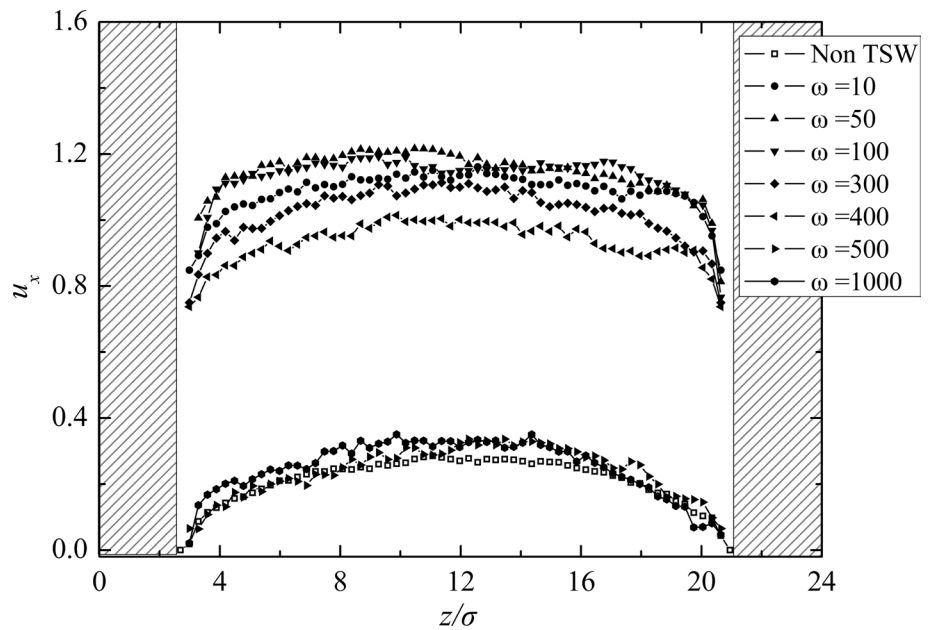


Fig. 11 Effect of frequency of travelling surface waves on velocity profiles



nanoscales Xie and Cao (2017). The influence of surface wettability of nanochannel walls on the velocity profile is shown in Fig. 15. As shown in Fig. 15, three magnitudes of FWI are considered, i.e. $c = 0.25, 0.5$ and 1.0 ($u_0 = 0.01$, $\omega = 10$, and g in the range of $0.01-0.025$), which refer to as the weak (hydrophobic), medium and strong (hydrophilic) interactions between fluid molecules and wall atoms, respectively. Figure 15a indicates that the difference of velocity profiles between the media and strong fluid–wall interactions under the small acceleration factor ($g = 0.01$) is insignificant with/without travelling surface waves on the walls. However, the difference between medium and strong

interactions is easily seen as the acceleration increases. In addition, the velocity profile becomes wider and velocity slip gets larger under the weak FWI (hydrophobicity), i.e. $c = 0.25$, which is shown in Fig. 15b–d. Moreover, the influence of FWI on the flow rate has also been obtained, and the flow rate ratio as a function of the acceleration factor with respect to the surface wettability is shown in Fig. 16. It is shown in Fig. 16 that the flow rate ratio is decreased under three magnitudes of fluid–wall interactions as the acceleration increases. In particular, the flow rate ratio under both medium and strong fluid–wall interactions (hydrophilicity) is larger than that under the weak

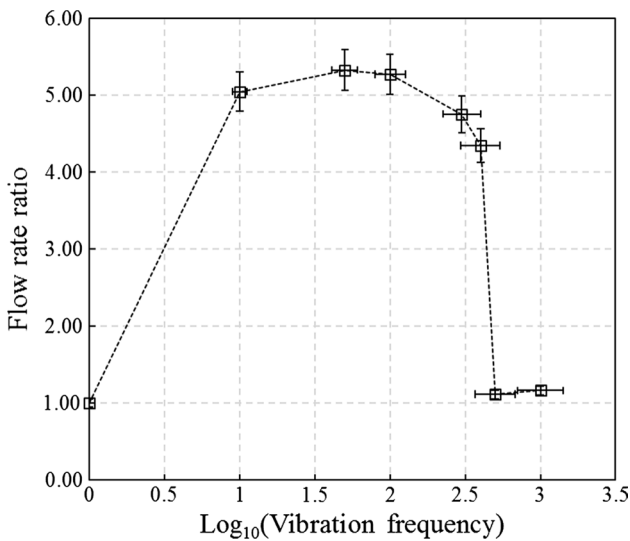


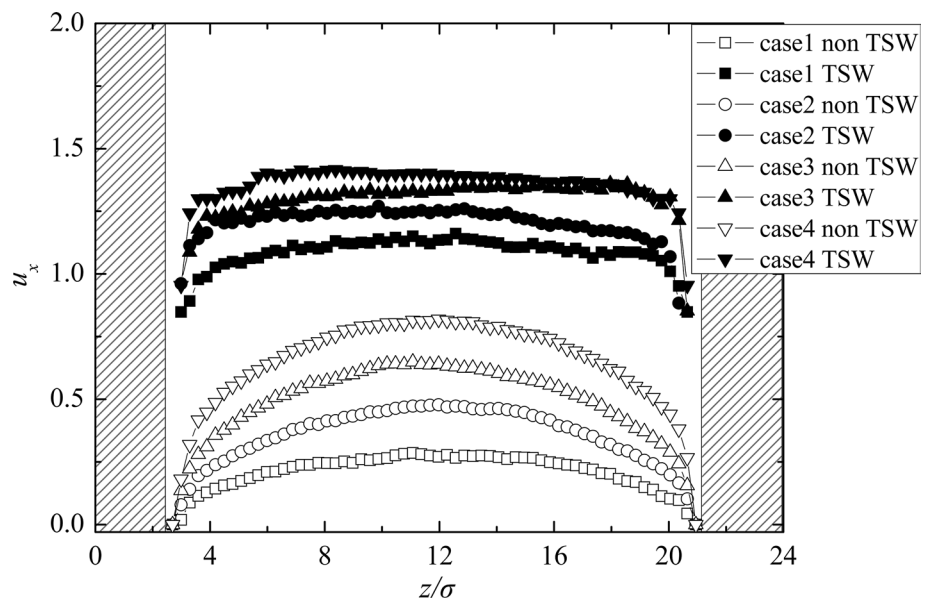
Fig. 12 Flow rate ratio as a function of frequency of travelling surface waves

fluid–wall interaction (hydrophobicity) with the increment in the acceleration. In addition, the maximum velocity of fluids across the nanochannel as a function of the acceleration factor is shown in Fig. 17, which indicates that the maximum velocity is proportional to the acceleration, i.e. the body force is really balanced by the shear stress in the nanochannel flow.

Recall that the condensed layer of fluid molecules near the nanochannel wall is destroyed by the travelling surface wave, and we expect that the viscosity of fluid in the nanochannel may also be affected by the travelling surface wave. In order to obtain the viscosity of fluid,

a second-order polynomial is applied to fit the velocity profile in the form of $u(z) = a_2z^2 + a_1z + a_0$. Then, we use the coefficient a_2 in the second-order polynomial to calculate the viscosity μ in terms of $\mu = -\rho g/2a_2$, i.e. Eq. (1). In addition, Ghorbanian and Beskok (2016) have proposed a further computation of fluid viscosity as follows. They use the maximum velocity, u_{max} , that occurs at the centre of nanochannels and find a coefficient a_2 from $u(z) = a_2z(z - H)$ as $a_2 = -\left|\frac{4u_{max}}{H^2}\right|$ and then calculate viscosity using the same formula $\mu = -\rho g/2a_2$ as investigators usually do. As a result, they have defined the fluid viscosity as the average of the two values. Based on the procedure presented above, the distribution of fluid viscosity with respect to the acceleration is shown in Fig. 18. As shown in Fig. 18, the shear viscosity of fluid in nanochannels keeps almost constant indicating that the fluid remains newtonian, and is independent on the acceleration factor without applying travelling surface waves. However, the viscosity of fluid is increased significantly as the wetting surface becomes hydrophilic, i.e. strong FWI, which is consistent with the observation by Liakopoulos et al. (2016) that the shear viscosity past a wall shows a monotonic increase with increased hydrophilicity. In particular, the viscosity under the small acceleration is slightly greater than that under the larger acceleration for three FWIs. Furthermore, it gets complicated for the viscosity of fluid when travelling surface waves propagate on the walls of nanochannels. Figure 18 shows that the fluid viscosity in the presence of travelling surface waves becomes greater than without applying travelling surface waves, and the increase in viscosity is more significant for hydrophobic interaction. The fluid viscosity on the hydrophilic surface, however, is insensitive to the

Fig. 13 Effect of acceleration factor on velocity profiles under travelling surface waves: case 1 $g = 0.01$; case 2 $g = 0.015$; case 3 $g = 0.02$; and case 4 $g = 0.025$



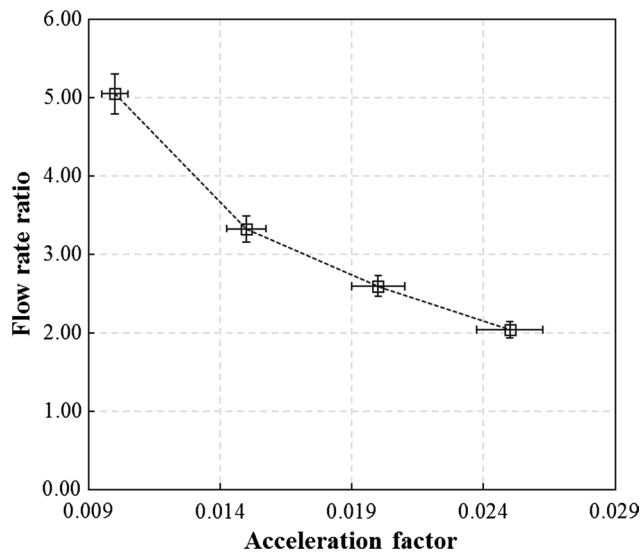


Fig. 14 Flow rate ratio as a function of acceleration factor under travelling surface waves

travelling surface wave and is only increased slightly. In addition, the increase in viscosity is obviously seen under the large acceleration: the increase is up to 70% or 40% on the hydrophobic surface and 10% on the hydrophilic surface, respectively. Raviv et al. (2002) analysed the ultra-thin water films confined between hydrophilic surfaces and found that the effective viscosity of water remains comparable to its bulk value even when it is confined to sub-nanometre thin films. It is confirmed in Fig. 18 that the increased viscosity of fluid induced by travelling surface waves also remains close to its value on the hydrophilic surface.

It is well known that the boundary slip always decreases the surface friction mainly depending on the ratio of the slip length and the characteristic length of the flow system, i.e. a dimensionless slip length Cao et al. (2006b). The slip effect becomes very important in micro-/nanoscale flows as the characteristic length decreases, such as nanochannel flows. That is, reducing the surface friction needs large slip length at the boundary. The velocity slip and slip length at micro-/nanoscale flows have been significantly affected by the surface conditions such as the surface roughness, nanostructured surface or permeable surface Yang (2006), Cao (2007), Somers et al. (2012), Xie and Cao (2016). Generally speaking, the friction of fluid flow past the solid wall will be reduced if the slip velocity takes place on the surface. However, the fundamental of the friction on the walls is less understood when the fluid flows through nanochannels in the presence of travelling surface waves. Thus, we are to determine the friction of nanoflows when the travelling surface waves propagate on the walls of

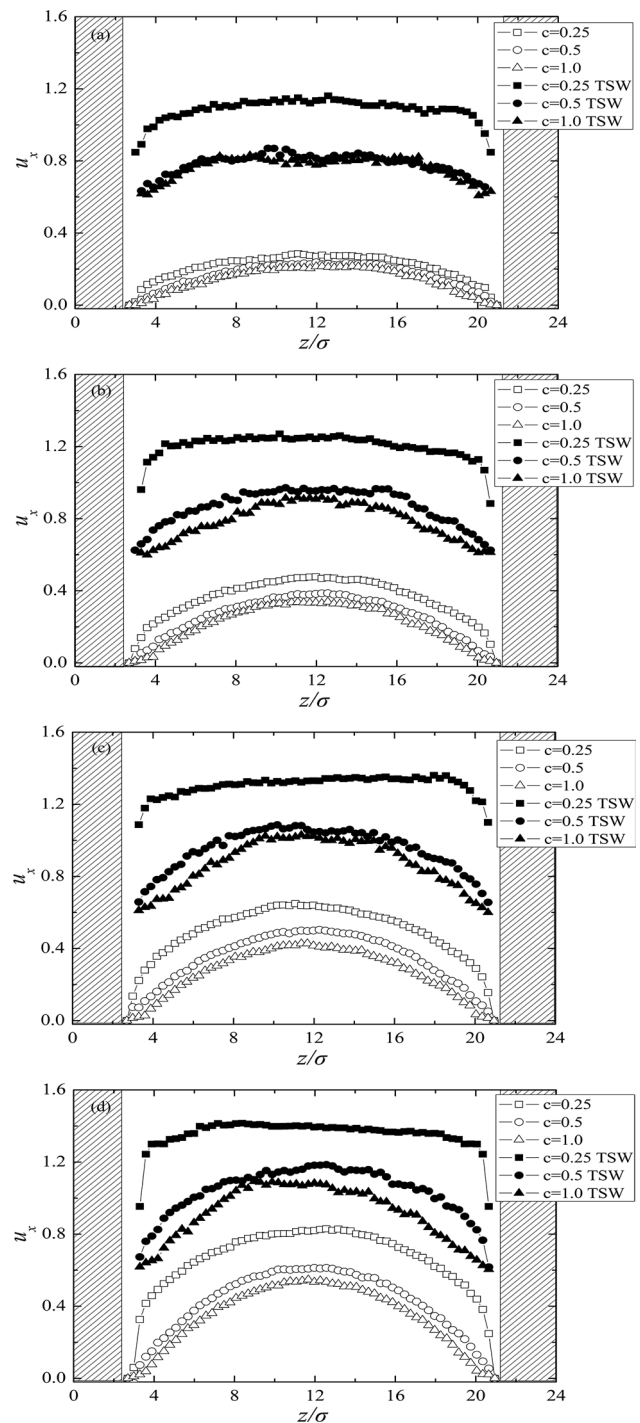


Fig. 15 Effect of the fluid–wall interactions on velocity profiles under different acceleration factors: **a** $g = 0.01$; **b** $g = 0.015$; **c** $g = 0.02$; and **d** $g = 0.025$

nanochannels. Take the case of force-driven flow for an example, and the friction coefficient, which characterizes the flow drag, can be written as

$$f = \frac{48}{\text{Re}} \frac{1}{1 + 6(L_s H)} \tag{8}$$

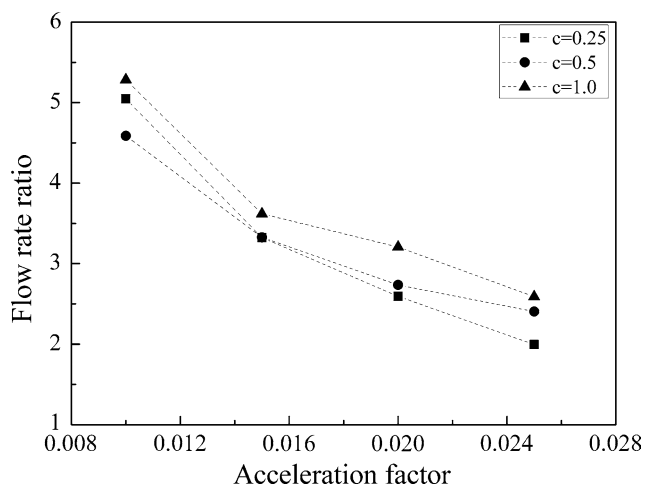


Fig. 16 Effect of the fluid–wall interactions on flow rate ratio under different acceleration factors. The *dotted lines* are used to guide the eye

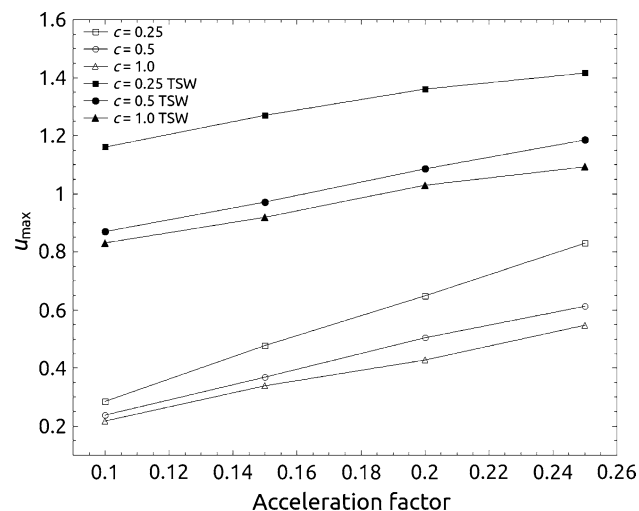


Fig. 17 Variation of the maximum velocity as a function of the acceleration factor

On the base of the slip length, which is calculated by extrapolating the velocity profiles, we have obtained the variety of friction coefficient on the wall as a function of the acceleration factor under travelling surface waves. The product of the friction coefficient f and the Reynolds number Re is often referred to as the friction constant $C_f = fRe$, and its reduction is shown in Fig. 19. As shown in Fig. 19, the reduction in friction coefficient on the wall falls slightly and then keeps the level under the weak FWI (hydrophobic surface) as the acceleration increases. However, the reduction in friction coefficient under both medium and strong FWI (hydrophilic surface) jumps up significantly as the acceleration increases, but

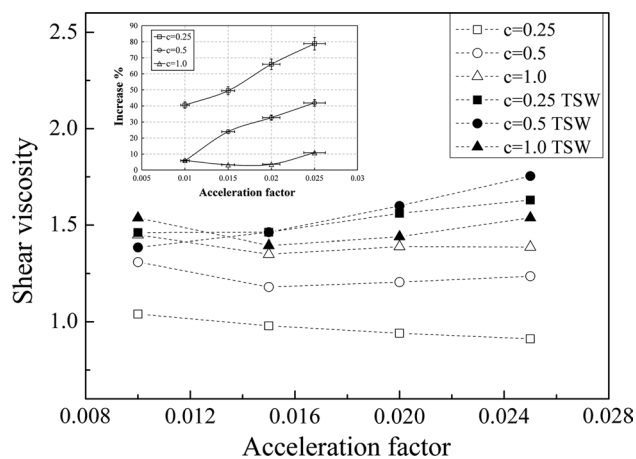


Fig. 18 Viscosity of fluid induced by travelling surface waves under three magnitudes of FWI. *Inset* the increase in viscosity as a function of acceleration

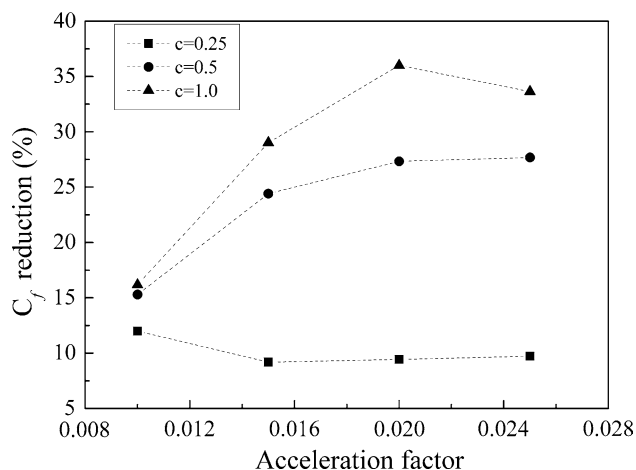


Fig. 19 Reduction in friction coefficient on the wall as a function of pressure gradient under travelling surface waves

drops slightly and keeps the level on the hydrophobic surface, respectively. It can be concluded that the surface friction on the wall of nanochannels is reduced significantly under both the medium and strong FWI (hydrophilic surface) in the presence of travelling surface waves in comparison with the weak FWI (hydrophobic surface). Previous works had also investigated the relationship between the slip length and viscosity of fluids. For example, Lichter et al. (2007) presented a linear dependence of the slip length on the liquid viscosity in their MD simulations, which reached an agreement with the experimental data Priezjev and Troian (2004). Moreover, Craig et al. (2001) reported that the slip length increases with the increase in viscosity of liquids. In our investigations, the increased viscosity of fluid induced by travelling surface waves in nanochannels contributes to a large slip length

on the wall resulting in the apparent reduction in surface friction.

4 Conclusion

In this paper, the fast flow has been observed in nanochannels in the presence of travelling surface waves. Both amplitude and frequency of travelling surface waves have influenced the nanoscale fluid dynamics of flow in nanochannels. The velocity profile got widened and flat under large amplitudes of travelling surface waves, indicating that the average flow velocity across the nanochannel was increased. Accordingly, the flow rate in nanochannels had been enhanced and was a monotonically increasing function of the amplitude of travelling surface waves, and a sevenfold increase in flow rate was observed. However, the flow rate had been only enhanced in the limited range of frequency of travelling surface waves such as low frequencies, and a maximum fivefold increase in flow rate was pronounced. As a force-driven flow, the flow rate was decreased as the acceleration increases. The fluid–wall interactions (surface wettability) also played an important role in flows through the nanochannels, and the flow rate had been enhanced significantly under the strong fluid–wall interaction (hydrophilicity) in the presence of travelling surface waves in comparison with the weak fluid–wall interaction (hydrophobicity). As a result, the surface friction on the wall of nanochannels was significantly reduced under both medium and strong fluid–wall interactions (hydrophilic surface), and the shear viscosity of fluid in nanochannels was increased in the presence of travelling surface waves on the hydrophobic surface. It can be concluded that our results open the potential strategies for the fast nanofluidics by travelling surface waves.

Acknowledgements The authors thank the reviewers for their constructive comments. JFX also thanks Professor Long Yu from Northwestern Polytechnical University for the useful discussions about the Rayleigh waves. The support of the National Natural Science Foundation of China (Grants No. 51506110 and 51676108) and Science Fund for Creative Research Groups (No. 51621062) was gratefully acknowledged.

References

- Allen MP, Tildesley DJ (1987) Computer simulation of liquids. Clarendon, Oxford
- Arash B, Jiang JW, Rabczuk T (2015) A review on nanomechanical resonators and their applications in sensors and molecular transportation. *Appl Phys Rev* 2:021301
- Barisik M, Beskok A (2011) Equilibrium molecular dynamics studies on nanoscale-confined fluids. *Microfluid Nanofluid* 11:269–282
- Bhadoria R, Aluru NR (2013) A quasi-continuum hydrodynamic model for slit shaped nanochannel flow. *J Chem Phys* 139:074109

- Bocquet L, Barrat J-L (1996) Hydrodynamic properties of confined fluids. *J Phys Condens Matter* 8:9297
- Bocquet L, Tabeling P (2014) Physics and technological aspects of nanofluidics. *Lab Chip* 14:3143–3158
- Brenker JC, Collins DJ, Van Phan H, Alan T, Neild A (2016) On-chip droplet production regimes using surface acoustic waves. *Lab Chip* 16:1675–1683
- Cao BY (2007) Non-Maxwell slippage induced by surface roughness for microscale gas flow: a molecular dynamics simulation. *Mol Phys* 105:1403–1410
- Cao BY, Chen M, Guo ZY (2005) Temperature dependence of the tangential momentum accommodation coefficient for gases. *Appl Phys Lett* 86:091905
- Cao B-Y, Chen M, Guo Z-Y (2006a) Liquid flow in surface-nanostructured channels studied by molecular dynamics simulation. *Phys Rev E* 74:066311
- Cao B-Y, Chen M, Guo Z-Y (2006b) Effect of surface roughness on gas flow in microchannels by molecular dynamics simulation. *Int J Eng Sci* 44:927–937
- Cao B-Y, Sun J, Chen M, Guo Z-Y (2009) Molecular momentum transport at fluid-solid interfaces in MEMS/NEMS: a review. *Int J Mol Sci* 10:4638–4706
- Capozza R, Vanossi A, Vezzani A, Zapperi S (2009) Suppression of friction by mechanical vibrations. *Phys Rev Lett* 103:085502
- Cecchini M, Girardo S, Pisignano D, Cingolani R, Beltram F (2008) Acoustic-counterflow microfluidics by surface acoustic waves. *Appl Phys Lett* 92:104103
- Craig VSJ, Neto C, Williams DRM (2001) Shear-dependent boundary slip in an aqueous newtonian liquid. *Phys Rev Lett* 87:054504
- Craighead H (2006) Future lab-on-a-chip technologies for interrogating individual molecules. *Nature* 442:387–393
- Daw R, Finkelstein J (2006) Lab on a chip. *Nature* 442:367
- Ding X, Li P, Lin S-CS, Stratton ZS, Nama N, Guo F, Slotcavage D, Mao X, Shi J, Costanzo F, Huang TJ (2013) Surface acoustic wave microfluidics. *Lab Chip* 13:3626–3649
- Friend JR, Yeo LY (2011) Microscale acoustofluidics: Microfluidics driven via acoustics and ultrasonics. *Rev Mod Phys* 83:647–704
- Gad-el-Hak M (1999) The fluid mechanics of microdevices—the free-man scholar lecture. *J Fluids Eng Trans ASME* 121:5–33
- Ghorbanian J, Beskok A (2016) Scale effects in nano-channel liquid flows. *Microfluid Nanofluid* 20:1–11
- Ghorbanian J, Celebi AT, Beskok A (2016) A phenomenological continuum model for force-driven nano-channel liquid flows. *J Chem Phys* 145:184109
- Giannakopoulos AE, Sofos F, Karakasidis TE, Liakopoulos A (2014) A quasi-continuum multi-scale theory for self-diffusion and fluid ordering in nanochannel flows. *Microfluid Nanofluid* 17:1011–1023
- Grest GS, Kremer K (1986) Molecular-dynamics simulation for polymers in the presence of a heat bath. *Phys Rev A* 33:3628–3631
- Guo YJ, Lv HB, Li YF, He XL, Zhou J, Luo JK, Zu XT, Walton AJ, Fu YQ (2014) High frequency microfluidic performance of LiNbO₃ and ZnO surface acoustic wave devices. *J Appl Phys* 116:024501
- Guttenberg Z, Rathgeber A, Keller S, Rädler JO, Wixforth A, Kostur M, Schindler M, Talkner P (2004) Flow profiling of a surface-acoustic-wave nanopump. *Phys Rev E* 70:056311
- Ho CM, Tai YC (1996) Review: MEMS and its applications for flow control. *J Fluids Eng Trans ASME* 118:437–447
- Ho CM, Tai YC (1998) Micro-electro-mechanical-systems (MEMS) and fluid flows. *Annu Rev Fluid Mech* 30:579–612
- Insepov Z, Wolf D, Hassanein A (2006) Nanopumping using carbon nanotubes. *Nano Lett* 6:1893–1895
- Irving J, Kirkwood J (1950) The statistical mechanical theory of transport processes. IV. The equations of hydrodynamics. *J Chem Phys* 18:817–829

- Kazakia JY, Rivlin RS (1978) Influence of vibration on Poiseuille flow of a non-Newtonian fluid. I. *Rheol Acta* 17:210–226
- Kazakia JY, Rivlin RS (1979) Influence of vibration on Poiseuille flow of a non-Newtonian fluid. II. *Rheol Acta* 18:244–255
- Koplik J, Banavar JR (1995) Continuum deductions from molecular hydrodynamics. *Annu Rev Fluid Mech* 27:257–292
- Koplik J, Banavar JR, Willemsen JF (1989) Molecular-dynamics of fluid-flow at solid-surfaces. *Phys Fluids A* 1:781–794
- Koster D (2007) Numerical simulation of acoustic streaming on surface acoustic wave-driven biochips. *SIAM J Sci Comput* 29:2352–2380
- Liakopoulos A, Sofos F, Karakasidis TE (2016) Friction factor in nanochannel flows. *Microfluid Nanofluid* 20:24
- Liang T, Ye W (2014) An efficient hybrid DSMC/MD algorithm for accurate modeling of micro gas flows. *Commun Comput Phys* 15:246–264
- Lichter S, Martini A, Snurr RQ, Wang Q (2007) Liquid slip in nanoscale channels as a rate process. *Phys Rev Lett* 98:226001
- Mao ZM, Xie YL, Guo F, Ren LQ, Huang PH, Chen YC, Rufo J, Costanzo F, Huang TJ (2016) Experimental and numerical studies on standing surface acoustic wave microfluidics. *Lab Chip* 16:515–524
- Morris DL, Hannon L, Garcia AL (1992) Slip length in a dilute gas. *Phys Rev A* 46:5279–5281
- Nama N, Barnkob R, Mao ZM, Kahler CJ, Costanzo F, Huang TJ (2015) Numerical study of acoustophoretic motion of particles in a PDMS microchannel driven by surface acoustic waves. *Lab Chip* 15:2700–2709
- Piau JM, Piau M (2002) Easier flow of viscoplastic materials with ultrasonic longitudinal wall motion. *J Nonnewton Fluid Mech* 104:185–226
- Priezjev NV, Troian SM (2004) Molecular origin and dynamic behavior of slip in sheared polymer films. *Phys Rev Lett* 92:018302
- Rapaport DC (1995) *The art of molecular dynamics simulation*. Cambridge University Press, Cambridge
- Raviv U, Giasson S, Frey J, Klein J (2002) Viscosity of ultra-thin water films confined between hydrophobic or hydrophilic surfaces. *J Phys Condens Matter* 14:9275
- Roosta S, Nikkiah SJ, Sabzali M, Hashemianzadeh SM (2016) Molecular dynamics simulation study of boron-nitride nanotubes as a drug carrier: from encapsulation to releasing. *RSC Adv* 6:9344–9351
- Shilton RJ, Travaglini M, Beltram F, Cecchini M (2014) Microfluidic pumping through miniaturized channels driven by ultra-high frequency surface acoustic waves. *Appl Phys Lett* 105:074106
- Somers J, He YL, Tao WQ, Rose JW, Wang HS (2012) Multi-scale study of liquid flow in micro/nanochannels: effects of surface wettability and topology. *Microfluid Nanofluid* 12:991–1008
- Thompson PA, Robbins MO (1989) Simulations of contact line motion: slip and the dynamic contact angle. *Phys Rev Lett* 63:766–769
- Thompson PA, Troian SM (1997) A general boundary condition for liquid flow at solid surfaces. *Nature* 389:360–362
- Worden K (2001) Rayleigh and Lamb Waves—basic principles. *Strain* 37:167–172
- Xie J-F, Cao B-Y (2016) Nanochannel flow past permeable walls via molecular dynamics. *AIP Adv* 6:075307
- Xie J-F, Cao B-Y (2017) Effects of surface conditions on nanochannel flow past permeable walls. *Mol Simul* 43:65–75
- Yang SC (2006) Effects of surface roughness and interface wettability on nanoscale flow in a nanochannel. *Microfluid Nanofluid* 2:501–511
- Yeo LY, Friend JR (2009) Ultrafast microfluidics using surface acoustic waves. *Biomicrofluidics* 3:012002
- Zhou J, DeMiguel-Ramos M, Garcia-Gancedo L, Iborra E, Olivares J, Jin H, Luo JK, Elhady AS, Dong SR, Wang DM, Fu YQ (2014) Characterisation of aluminium nitride films and surface acoustic wave devices for microfluidic applications. *Sens Actuators B Chem* 202:984–992
- Zhou X, Wu F, Liu Y, Kou J, Lu H, Lu H (2015) Current inversions induced by resonant coupling to surface waves in a nanosized water pump. *Phys Rev E* 92:053017
- Ziarani AS, Mohamad AA (2006) A molecular dynamics study of perturbed Poiseuille flow in a nanochannel. *Microfluid Nanofluid* 2:12–20